



HAL
open science

Assessment of pebble virtual velocities by combining active RFID fixed stations with geophones

Mathieu Cassel, Oldrich Navratil, Frédéric Liébault, Alain Recking, Daniel Vázquez-Tarrío, Maarten Bakker, Sébastien Zanker, Clément Misset, Hervé Piégay

► To cite this version:

Mathieu Cassel, Oldrich Navratil, Frédéric Liébault, Alain Recking, Daniel Vázquez-Tarrío, et al.. Assessment of pebble virtual velocities by combining active RFID fixed stations with geophones. *Earth Surface Processes and Landforms*, 2023, 48 (13), pp.2570-2583. 10.1002/esp.5646 . hal-04293682

HAL Id: hal-04293682

<https://hal.science/hal-04293682>

Submitted on 25 Jan 2024

HAL is a multi-disciplinary open access archive for the deposit and dissemination of scientific research documents, whether they are published or not. The documents may come from teaching and research institutions in France or abroad, or from public or private research centers.

L'archive ouverte pluridisciplinaire **HAL**, est destinée au dépôt et à la diffusion de documents scientifiques de niveau recherche, publiés ou non, émanant des établissements d'enseignement et de recherche français ou étrangers, des laboratoires publics ou privés.



Distributed under a Creative Commons Attribution - NonCommercial - NoDerivatives 4.0 International License

Assessment of pebble virtual velocities by combining active RFID fixed stations with geophones

Mathieu Cassel¹  | Oldrich Navratil²  | Frédéric Liébault³  | Alain Recking³  | Daniel Vázquez-Tarrío⁴  | Maarten Bakker³  | Sébastien Zanker⁵ | Clément Misset⁶ | Hervé Piégay¹ 

¹EVS, ENS of Lyon, UMR 5600 CNRS, Lyon, France

²EVS, Lyon 2, UMR 5600 CNRS, Lyon, France

³Université Grenoble Alpes, INRAE, CNRS, IRD, Grenoble INP, IGE, 38000 Grenoble, France

⁴Universidad Complutense de Madrid. Departamento de Geodinámica, Estratigrafía y Paleontología, Madrid, Spain

⁵EDF, DTG, Grenoble, France

⁶ONF-RTM, Northern Alps Agency, Chambéry, France

Correspondence

Mathieu Cassel, UMR 5600 CNRS-Environnement Ville Société, ENS de Lyon, University of Lyon, Lyon Cedex, France.
Email: casselmathieu@gmail.com

Funding information

This work was carried out as part of the project Greendam, which is an original partnership integrating an inter-disciplinary scientific group (EVS UMR 5600 and SiSyPh UMR5672 du CNRS et INRAE), a large electricity producer (Électricité de France - EDF), and a local SME (GeoPeka), as part of a partnership project with the Région Auvergne-Rhône-Alpes.; This work was performed within the framework of the EUR H2O²Lyon (ANR-17-EURE-0018) of Université de Lyon, part of the program "Investissements d'Avenir" (ANR-11-IDEX-0007) operated by the French National Research Agency (ANR).

Abstract

Monitoring bedload transport in rivers is a challenging research domain teeming with technical innovations and methodological developments aimed at improving our knowledge and models of bedload processes at different spatial-temporal scales. Radio frequency identification (RFID) technology has improved sediment tracking, allowing the characterisation of transport processes of individual particles at flood-event scales. Meanwhile, geophone sensors have enabled the long-term continuous monitoring of seismic signals that can provide surrogate measures of bedload fluxes at local scales, during flood events and at sediment-pulses. The combination of these two techniques could allow sediment transport processes to be linked with both flood events and sediment pulses. In this study, we used a combination of active ultra-high frequency RFID technology and geophone monitoring stations to link the virtual velocity of tracers with seismic activity, hydraulic forcing, and the properties of the tracked particles. Single and multiple regression models show that seismic activity best explained the observed variance (81%) of the virtual velocity of particles, in comparison with discharge (58%) and stream power (63%). Furthermore, when several control variables (seismic activity and particle properties) were combined in an empirical model, the model explained 89% of the variance and allowed quantification of the portions of the variance explained by hydraulic forcing, geophonic activity and tracked particles. These results show the high potential of these combined monitoring techniques for future in-field experiments to investigate bedload processes at different spatiotemporal scales in rivers of different morphologies.

KEYWORDS

Alpine stream monitoring, bedload transport, geophone monitoring, pebble virtual velocity, RFID pebble tracking

1 | INTRODUCTION

Although bedload transport processes are important in flood hazard assessment, engineering applications and river ecology, our understanding of these processes remains limited, making them difficult to predict (Ancey, 2020a, 2020b; Gomez, 1991; Recking, 2013). The study of bedload transport processes has been accomplished through

two main approaches or research frameworks: Lagrangian and Eulerian approaches. The former seeks to follow the motion and dispersion of individual particles (usually within a finite spatial domain), whereas the second measures the dynamics of sediment fluxes at a prescribed location (Ballio et al., 2018). In order to better understand the complexity of bedload processes and the dynamics of individual particles add up to bedload dynamics in rivers, it is essential to use

This is an open access article under the terms of the [Creative Commons Attribution-NonCommercial-NoDerivs](https://creativecommons.org/licenses/by-nc-nd/4.0/) License, which permits use and distribution in any medium, provided the original work is properly cited, the use is non-commercial and no modifications or adaptations are made.

© 2023 The Authors. *Earth Surface Processes and Landforms* published by John Wiley & Sons Ltd.

both of these forms to provide alternative descriptions of the same process. However, the field monitoring of bedload transport during rare and intense flood events still remains challenging, whether in coarse-bedded gravel rivers, steep-slope torrents (Rickenmann, 2017) or large rivers. Therefore, the development of new tools and methods is important to gain insights into the contributions of the different factors controlling bedload transport (Kondolf & Piégay, 2016). Among the recent field monitoring developments, active ultra-high frequency transponders (a-UHF tags), radio frequency identification (RFID) and seismic sensors (SS) are emerging techniques, each feeding one of the Lagrangian (a-UHF) and Eulerian (SS) approaches introduced above.

Over the last few decades, RFID technology with wireless detection of individual (buried or immersed) transponder-equipped particles has been used to investigate the movement of individual coarse sediment particles and determine how such movement depends on hydraulic forcing, river system morphodynamics, channel geometry, and particle properties (Hassan & Bradley, 2017; Vázquez-Tarrío & Batalla, 2019). Hydraulic forcing is often considered using the mean flow discharge and/or the stream power above the critical level for incipient particle motion (Bagnold, 1966; Shields, 1936). Many studies have developed empirical models based on the barycenter of particle plumes, modeling the downstream progression (Arnaud et al., 2017; Chardon et al., 2021; Vázquez-Tarrío et al., 2023), dispersion (Haschenburger, 2013) and virtual velocity (Haschenburger & Church, 1998; Liébault et al., 2012) as functions of excess stream power (Arnaud et al., 2017; Chardon et al., 2021; Houbrechts et al., 2015; Lamarre & Roy, 2008; Rainato et al., 2020; Schneider et al., 2014) or stream impulse (Bradley, 2017; Gilet et al., 2020; Imhoff & Wilcox, 2016; Phillips et al., 2013; Phillips & Jerolmack, 2014) at flood-event scales. Within the same temporal scale, channel geometry is related to spatial and vertical heterogeneity in erosion and deposition processes (Haschenburger & Wilcock, 2003; Hassan & Bradley, 2017; McDowell & Hassan, 2020; Papangelakis & Hassan, 2016) and to alluvial macroforms that act as structural elements influencing channel morphology and dimensions (Vázquez-Tarrío & Batalla, 2019; Vázquez-Tarrío et al., 2021; Vázquez-Tarrío et al., 2019). At smaller spatial and temporal scales, a probabilistic approach is used to model the motion of individual particles, distinguishing phases of displacement and rest according to hop length and duration, and allowing the computing of probability curves for occurrences in both of these phases (Einstein, 1937; Ergenzinger & Schmidt, 1990; Habersack, 2001; Olinde & Johnson, 2015). However, small-scale turbulent flow processes and grain-grain interactions also remain of fundamental importance in bedload transport (Frey & Church, 2011), and their effects on coarse tracers transport have not yet been investigated in a field experiment. This may be partly because in-field experiments using stationary antennas detect RFIDs using low-frequency passive transponders (PIT tags) reported low recovery/detection rates (Mao et al., 2017; Schneider et al., 2010; Stähly et al., 2020). However, recent studies using sediment tracers equipped with a-UHF transponders exhibited encouraging results when the tracers were tracked with mobile reading system (Brousse, Arnaud-Fassetta, et al., 2020; Brousse, Liébault, et al., 2020; Cassel et al., 2020; Missset et al., 2020). Furthermore, Cassel, Navratil, et al. (2021) used an autonomous stationary antenna system (named e-RFIDuino) to measure particle

virtual velocity during flood events. This new approach opens new opportunities to link instantaneous particle mobility with geophonic signals.

Geophones are seismic sensors that can be installed on river banks and used to monitor bedload transport through the recording of seismic activity generated at the river bed. Bedload flux can be estimated from seismic power (Tsai et al., 2012) by taking into account the contributions of both water turbulence and bedload flux (Dietze et al., 2019) or by linking grain-scale impacts with seismic activity (Gimbert et al., 2019). Bakker et al. (2020) and Dietze et al. (2020) also performed in-field validations to estimate absolute bedload transport rates. Hence, geophones can be used to obtain surrogate measures for monitoring bedload flux in rivers and for investigating processes with high temporal variability because they can run quasi-continuously over a long-time period and can operate in high-magnitude flow events during which in-stream equipment is not likely to function correctly or may even be destroyed. Bedload samples are always necessary to calibrate the seismic records when investigating absolute bedload transport flux (Antoniazza et al., 2020; Bakker et al., 2020; Rickenmann et al., 2014), and these samples may be acquired with sediment traps or basket samplers (e.g. Helley Smith). Geophones have been used to study glacial lake outbursts (Cook et al., 2018), debris flow triggering in torrents (Bel et al., 2017; Navratil et al., 2013; Roth et al., 2017), gravel mobilisation (Schmandt et al., 2017), and bedload transport downstream of hydropower dams (Aigner et al., 2017) and in near-natural Alpine streams (Misset et al., 2020). Such monitoring programmes often combine geophone sensors with quantification of turbidity (Misset et al., 2021), flow rheological characterisation (Navratil et al., 2013), pluviometry (Bel et al., 2017), topographic survey (Cook et al., 2018; Schmandt et al., 2017) and bedload flux sampling (Aigner et al., 2017; Missset et al., 2020; Rickenmann et al., 2012), but they only rarely include sediment tracers (Habersack et al., 2010; Missset et al., 2020; Schneider et al., 2014), which until recently were only used to explore event-based transport conditions, and not instantaneous ones.

Following on the above-described methods, we felt that it was necessary to describe the links between bedload transport observations based on RFID tracers continuously monitored by fixed stations (Lagrangian approach) and geophonic sensors (Eulerian approach). Assuming that grain-grain (mobile vs mobile particles) and grain-bed (mobile vs immobile particles) interactions (i.e. collisions) are colinear and generate ground vibrations, seismic activity could be used to monitor these interactions (Tsai et al., 2012) and the data could then be linked to the measurements of displacement of individual particles. Thus, the signals from seismic sensors could be used to estimate tracer displacements through descriptions of the bedload intensity surrounding the particle surrounding bedload intensity. The displacements (velocity) of sediment tracers with known properties (especially mass) could also be linked to the seismic energy recorded during their passages. This concept combining both approaches should provide insights allowing bedload transport monitoring to be improved, and increase our understanding of how different controlling factors (i.e. bedload properties and hydraulic conditions) affect its dynamics.

The main objectives of this paper are (1) to explore the potential of these two distinct monitoring methods (i.e. a-UHF RFID stations

and geophones) in combination; (2) to compare the respective influences of the controlling factors (hydraulics, seismic and tracers properties) on the variance of virtual velocity of the tracers; and (3) to investigate the accuracy (using a least squares multiple regression model) of predictions of tracer virtual velocity made according to these controlling factors.

2 | STUDY SITE

The Séveraise River drains a watershed with low human influence in the Ecrins Massif, French Alps. It has a catchment area of about 223 km² (maximum elevation of 3579 m a.s.l.; minimum elevation of 780 m a.s.l.) and a length of 33.2 km. Along its course, it shows several sequences of well-developed braided reaches in wider sections of the valley and straight single-thread reaches in the more laterally confined sections (Misset et al., 2020). The upper part of the catchment is highly prone to sediment erosion and processes such as rock fall, debris flows and sediment transport from torrents deliver large amounts of sediment to the main channel. From late spring to the beginning of summer, the Séveraise River exhibits a hydrologic regime characterised by a high-flow period driven by snowmelt, with daily discharges able to mobilise coarse sediments. This is followed, during the summer, by generally lower flows generated by glaciers ice melt with occasional storm events that can cause large flood events with intense bedload transport. The lowest flows occur in winter when the basin is covered by snow. In this study, we consider the snowmelt period from May to 15 July 2020 and storm-driven events over the period from 15 July to November 2020.

Our study site is located in approximately the middle section of the river near the village of Villar-Loubière (44°49'28.34" North;

6°08'56.22" East), just upstream of a gauging station (Figure 1) that was installed in 1969, and represents a drainage area of ca. 130 km². In the vicinity of a bridge, the channel is straight, laterally confined, and 13 m wide (Bakker et al., 2020), with an average slope of 0.014 m m⁻¹. The riverbed is armored with cobbles of grain size D50 = 11 cm and D84 = 30 cm, as derived from Wolman pebble counts (Misset et al., 2020). Under the most frequent hydraulic conditions, the bedload fluxes generated in the upstream braiding section are transferred efficiently within this confined section, without morphological adjustments (Misset et al., 2020). The morphodynamically active upstream braided reach exhibits a finer grain size with D50 = 28 mm and D84 = 91 mm.

3 | MATERIALS AND METHODS

The present bedload monitoring programme combines pebble a-UHF equipped pebble tracers with geophone sensors recording vertical ground vibrations. The pebble tracing programme was progressively implemented between 2018 and 2020 to quantify the pebble transport and mobility within the braided reach over several years (see Misset et al., 2020).

3.1 | Bedload monitoring equipment

The straight section of the channel was chosen for to installation of most of the monitoring systems because its width (13 m) and lateral confinement made covering and sensing the entire channel width practical and ensured the safety of the permanent equipment during high flow periods.

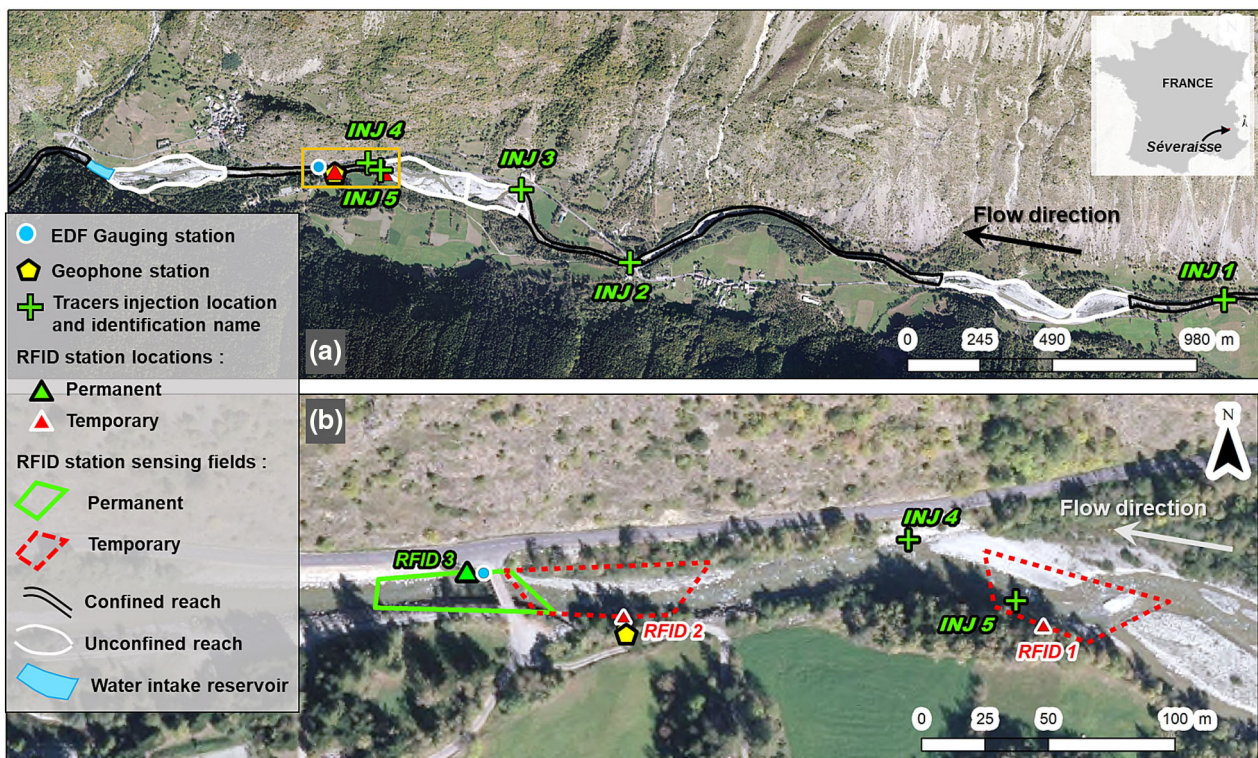


FIGURE 1 Overview of the (a) Séveraise River and the (b) monitoring instruments. [Color figure can be viewed at [wileyonlinelibrary.com](https://onlinelibrary.wiley.com)]

3.1.1 | Particle monitoring

Tracers

Over the course of 3 years, a total of 123 tracers were injected in 10 seeding operations at five different locations (Table 1 and Figure 1). Because of high water discharges at the seeding periods, the tracer injection consisted of dropping the tracers into the main channel flux, either from bridges (INJ 1 and INJ 2) or from banks (INJ 3, INJ 4 and INJ 5).

The tracers seeded at the beginning of the 2020 field campaign were artificial pebbles (Figure 2a) composed of a mixture of polyurethane resin and corundum (Cassel, Piégay, & Lavé, 2017; Cassel, Lavé, et al., 2021). They were equipped with active transponders of a-UHF tags. The a-UHF tags used in this study were COIN models developed by Ela Innovation® and distributed by Cipam®. These a-UHF tags were chosen because they have a relatively long operating life (up to 5 years) and can be sensed over dozens of meters (up to 40 m) in an open environment and over several meters when buried or immersed (up to

2.6 m). Their beacon signals are emitted at 433.9 MHz and do not suffer from collision when several transponders are simultaneously present in the antenna sensing field. The beacon signal also includes a received signal strength indication (RSSI) (Cassel, Dépret, & Piégay, 2017; Cassel et al., 2020). During the 2020 campaign, 29 new tracers equipped with COIN ID tags emitting a signal every 2.2 s were seeded.

Tracer monitoring stations

Three RFID-tracking stations were installed on-site on 28 May 2020, two being temporary and one, referred to as 'e-RFIDuino', being permanent (Cassel, Navratil, et al., 2021) (Figure 1b). When a tracer signal was sensed by an antenna, the stations recorded its identification number, the RSSI, and the timestamp. After the installation of the stations, the antenna sensing fields were delimited using the procedure detailed in Cassel, Navratil, et al. (2021). This ensured detection of the tracer's over the whole channel width and allowed us to determine the channel length over which the tracers could be monitored. A channel length of ~60 m was obtained for RFID 2 and RFID 3 (Figure 1b).

TABLE 1 Summary of the tracer seeding information.

Injection ID	ID of injection location	Date of seeding	Number of tracers injected	D50 (mm)	Number of tracers detected during the 2020 season at RFID stations: RFID 3 and RFID 2 (RFID 2 indicated in parentheses)
2	INJ 1	03/05/2019	20	68	2
5	INJ 2	27/05/2020	9	57.3	6
7	INJ 2	28/05/2020	10		8
8	INJ 5	02/06/2020	3		3 (3)
9	INJ 5	03/06/2020	5		5 (2)
10	INJ 5	04/06/2020	5		5 (1)
Total					31 (6)

Notes: In the rightmost column, the numbers in parentheses indicate the number of tracers sensed by station RFID 2. Injections 1, 3 and 4 are not presented here as the tracers seeded at these injections were either immobile or were already downstream of the reach investigated in this study.

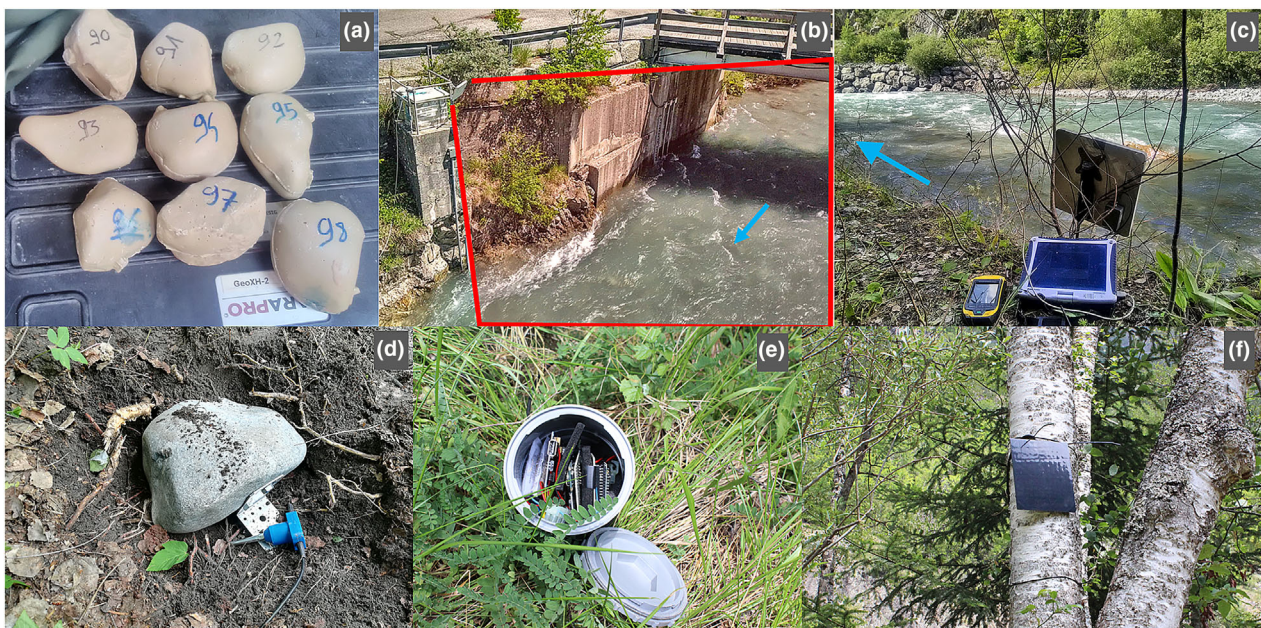


FIGURE 2 RFID devices, geophone station [(a) artificial tracers equipped with a-UHF tags; (b) e-RFIDuino station; (c) mobile RFID station 1], and geophone datalogger [(d) Geospace® GS-20DX geophone before its installation on a rock; (e) encapsulated datalogger for the geophone signal; (f) solar panel]. [Color figure can be viewed at wileyonlinelibrary.com]

The two temporary stations consisted of equipment used for mobile prospection surveys (Figure 2c): a rugged field computer connected to a SCIEL reader equipped with a SLENDER III antenna (see details in Cassel, Dépret, & Piégay, 2017; Cassel et al., 2020). The upstream temporary station was installed on the left bank at the location of the INJ 5 seeding point and was only used to observe the departure of the tracers seeded at this location. The downstream temporary station was installed as close as possible to the geophone station and was used to detect the tracers' passages and to monitor their displacement and the duration of their residency within the sensing field. These mobile stations were installed in the morning and removed at night when the tracers were injected at INJ 4 and INJ 5: on 28 May and 2–4 June.

The e-RFIDuino station consisted of an environmental Arduino based datalogger kitted out with a commercially available RFID reader (SCIEL reader) and a SLENDER III antenna (Figure 2b; see design details in Cassel, Navratil, et al., 2021). It was installed next to the EDF gauging station (Figure 1b), which provides flow discharge measurements (10-min time-step recording). The e-RFIDuino station remained on-site during the whole campaign (from 28 May until 26 October 2020). These three RFID stations allowed movement of the tracers to be quantified through monitoring of the virtual velocity of individual tracers (Einstein, 1937; Haschenburger & Church, 1998; Sayre & Hubbell, 1965), which is defined as the transport distance divided by the measurement interval. The data were analysed to link tracer movements to flow discharge, seismic activity, and tracer properties (shape and mass).

3.1.2 | Geophone monitoring stations

A geophone station was installed in a similar way to that described by Navratil et al. (2013) and Bel et al. (2017). The geophone station was powered by a small 3.7 V battery (10,000 mAh), a solar panel (3 W) and a solar power regulator. A microcontroller (Arduino Mini Pro[®]; 8 MHz) was chosen because of its very low energy consumption. An RTC (Real-Time Clock controller; RTC DS3231 AT24C32 IIC) and SD card reader (DEV13743) completed the recording system. A micro-SD memory card (8 Go) provided a data storage autonomy of several months. A GS20-DX Geospace[®] geophone (a natural frequency of 8 Hz) was deployed on the left riverbank ca. 2 m from the river flow. This geophone recorded ground vibration in the vertical direction. The vibration frequency typically associated with bedload transport is 50–60 Hz (Bakker et al., 2020), which meant that the maximum recording frequency of the microcontroller (5 Hz) was insufficient to record the output signal of the geophone, that is, a voltage proportional to the soil vibration velocity. To accommodate this problem, the raw geophone signal was first processed with an electronic interface that performed (1) a signal rectification, (2) low-pass filtering (frequency = 2.5 Hz), and (3) amplification of the geophone signal output, following the method of Navratil et al. (2013). The output signal was finally recorded at 5 Hz. The offset and gain of this interface can be adjusted to account for local ground properties and the specific location of each geophone. The geophone was fixed to a big boulder embedded in the riverbank (at 20-cm depth in the ground) to reduce the effects from direct impacts of rain, hail, and runoff, and the wires to the solar panel were fixed to eliminate noise induced by wind.

Finally, to define a gain value and verify that the station worked properly, preliminary drop tests were performed with boulders (ca. 10 kg) being manually thrown into the river (from 3 to 4 m in height) and onto the riverbanks (from 1.5 m), and these were clearly identified in the seismic record.

3.2 | Data computing

3.2.1 | Data compilation

The tracer properties were measured before they were seeded into the river. Each tracer was weighed, and its three axes were measured.

For each tracer passage (P_i) at one of the RFID stations (RFID 2 or RFID 3), we computed the virtual velocity (\bar{v}_{P_i}) expressed in m s^{-1} using the following formula:

$$\bar{v}_{P_i} = \frac{l}{t_{P_i}} = \frac{60 \text{ m}}{t(\text{exit})_{P_i} - t(\text{entry})_{P_i}}$$

with

- $l = 60 \text{ m}$, which is the channel length covered by the antenna sensing field (see Tracer monitoring stations section);
- t_{P_i} = tracer stay duration (in seconds) within the antenna sensing field, which is equal to the difference between the timestamps of entry (i.e. $t(\text{entry})_{P_i}$) and exit (i.e. $t(\text{exit})_{P_i}$) from the antenna sensing field.

The virtual velocity uncertainties were calculated using the following formula

$$\frac{\Delta \bar{v}_{P_i}}{\bar{v}_{P_i}} = \sqrt{\left(\frac{\Delta l}{l}\right)^2 + \left(\frac{\Delta t_i}{t_{P_i}}\right)^2}$$

with

- $\Delta l = 2 \text{ m}$ (1 m each for the upstream and downstream limits of the antenna sensing field);
- $l = 60 \text{ m}$, the channel length covered by the antenna sensing field;
- $\Delta t_i = 4.4 \text{ s}$: 2.2 s (the transponders signal emission interval) at both the entry and exit of the antenna sensing field;
- t_{P_i} = tracer stay duration (in seconds) within the antenna sensing field

We then used the timestamps (i.e. $t(\text{entry})_{P_i}$ and $t(\text{exit})_{P_i}$) of each tracer passage at an RFID station to derive (1) the flow discharge measured at the gauging station (Q , in $\text{m}^3 \text{ s}^{-1}$) and (2) the seismic activity (G , in mV) recorded at the geophone station (both are recorded at 10-min intervals). The Q and G value series were then used to calculate the mean values \bar{Q}_i and \bar{G}_i . The maximal values of Q and G were also calculated, but their links to virtual velocity were weaker than those of their mean values.

We investigated two stream power formulations commonly used in riverine pebble tracking, both of which include the tracer size in their computation:

- the sum of the unit excess flow power based on the discharge values exceeding the critical discharge for bedload transport (Q_c , estimated based on the 84th percentile of bed sediment size distribution), which is also considered as the total excess flow energy (Chardon et al., 2021; Haschenburger, 2013; Schneider et al., 2014);
- and the dimensionless stream power (Eaton & Church, 2011), which allows comparisons between contrasting river systems of different width, slope, and discharge regime, and avoids scale differences (Vázquez-Tarrio et al., 2019). It could thus be a good standard for further replications of the empirical models developed in this study.

The sum of the unit excess flow power ($\sum_t^{P_i} (\omega_t - \omega_c)$ in $W m^{-2}$) is suitable when several hydrological events are recorded by displacement of tracers between two surveys, or when the tracer residence duration in the antenna sensing field is long. It is the summed stay duration of each tracer passage P_i as

$$\sum_t^{P_i} (\omega_t - \omega_c) = \sum_t^{P_i} \frac{\rho \cdot g \cdot (Q_t - Q_c) \cdot S}{w} \quad (1)$$

where Q_t is the instantaneous discharges summed over the tracer's passage (P_i) duration to a resolution of 1 s; S and w are the straight confined channel slope ($0.014 m m^{-1}$) and width (13 m), respectively; ρ is the water density equal to $1000 kg m^{-3}$; and g is the acceleration due to gravity, which is equal to $9.81 m s^{-2}$. Bedload had been measured with an Elwha sampler over successive years, and the critical discharge for the entire bed mobility was known to be $11.9 m^3 s^{-1}$ (Bakker et al., 2020). This value is also consistent with the $11.7 m^3 s^{-1}$ estimated using the following equation derived from the Shields and Manning formulas:

$$Q_c = \left(K \cdot w \cdot S^{1/2} \right) \cdot \left(\left((1.65 \cdot D_{84} \cdot \tau_c^*) / S \right)^{3/5} \right) \quad (2)$$

where K is the Manning-Strickler coefficient equal to 26, calculated using the Strickler (1923) formula: $K = \frac{1}{n} = \frac{21}{D_{84}^{1/6}}$, D_{84} is the 84th

percentile of the tracers b -axis values (0.303 m), and τ_c^* is the critical Shields number (0.045).

The dimensionless stream power (ω^*) proposed by Eaton & Church (2011) is calculated as

$$\omega^* = \frac{\bar{\omega}}{\rho \cdot (g \cdot R \cdot D)^{3/2}} \quad (3)$$

where $\bar{\omega} = (\rho \cdot g \cdot S \cdot \bar{Q}_i) / w$ is the unit stream power (ω in $W m^{-2}$), as defined by Bagnold (1966, 1980), and estimated at the mean value of the discharge \bar{Q}_i observed during the passage of the tracers P_i . R is the submerged specific weight of the tracer (1.65), and D_i is the tracer b -axis value in m. The dimensionless stream power is linearly dependent on the mean value of the discharge.

3.2.2 | Data analysis

The data were processed and analysed using R and Rstudio statistical software (<http://www.rstudio.com/>). All the variables (virtual velocity and their potential drivers) were log-transformed. We first determined how much of the variance in the tracers' virtual velocity (during their passages) could be explained by each of the potential drivers in Table 2 and computed the raw correlation matrix using the 'cor (method = Spearman)' function in Rstudio.

Then, the correlations of the averaged seismic activity with the mean flow discharge and the dimensionless stream power were analysed using multiple R-squared coefficients obtained with the 'lm()' function in Rstudio.

Finally, using (i) log transformed seismic averaged values (\bar{G}_i), and the particle (ii) mass (m_i) and (iii) sphericity (Ψ_i), we developed an empirical model to predict the virtual velocity of tracers. Log transformer values of these drivers were processed using multiple least squares regression to adjust a log-log power model in a linearised form (also using the 'lm()' function in Rstudio). We also tested the potential contribution of ϵ_i to improving the model, with being ϵ_i the residuals from the power model linking log transformed dimensionless mean stream power (ω^*) and log transformed seismic averaged values (\bar{G}).

TABLE 2 Description of the control factors tested to predict particle virtual velocity.

Factor type	Description	Code variable	Included in MLS model
Tracers properties	Mass in kg	m_i	Yes
	Sphericity based on Sneed & Folk (1958) index: $I = \sqrt[3]{\frac{c}{ab}}$ with a , b , and c the longest, intermediate, and shortest axes of the tracer, respectively.	Ψ_i	Yes
Hydrological and hydraulic variables	Water discharge in $m^3 s^{-1}$. This is the mean value of the discharges measured during the tracer passage.	\bar{Q}_i	No
	Sum of the unit excess flow power in $W m^{-2}$	$\sum_t^{P_i} (\omega_t - \omega_c)$	No
	Dimensionless mean stream power	ω^*	No
Geophonic variables	Average geophone activity observed during the passage of the tracer in mV.	\bar{G}_i	Yes
	The residuals from the power model linking log transformed dimensionless mean stream power (ω^*) and log transformed seismic averaged values (\bar{G})	ϵ_i	Yes

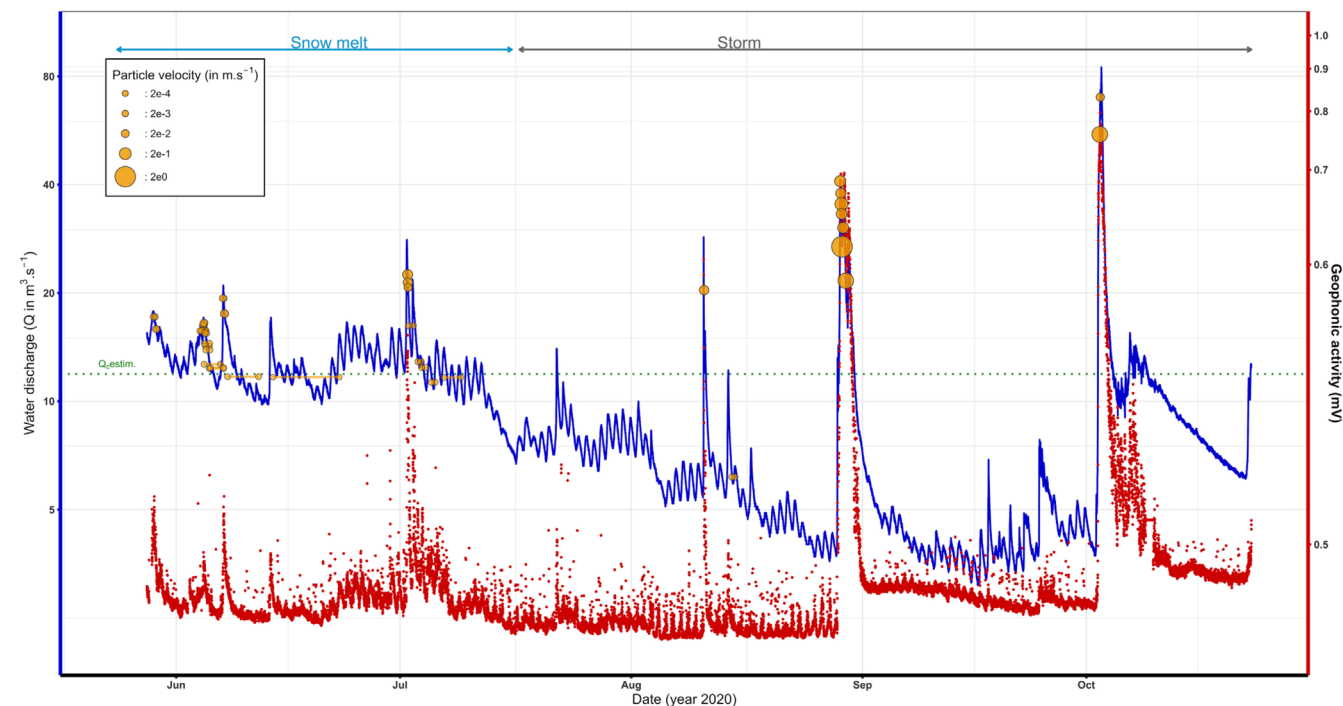


FIGURE 3 Discharge, seismic activity and the 37 tracer passages at the RFID stations ‘RFID 2’ and ‘FID 3’ during the 2020 season. Notes: Q_c is estimated at $11.9 \text{ m}^3 \text{ s}^{-1}$. The blue curve indicates discharge values reported on the left logged ordinate axis. Red dots represent geophonic activity values reported on the right logged ordinate axis. Orange circles indicate tracer passages during the snowmelt- and storm-driven floods, and their sizes are proportional to the virtual velocity. Orange horizontal segments indicate the residence time of the tracers within the sensing field of the RFID antennas. [Color figure can be viewed at wileyonlinelibrary.com]

4 | RESULTS

4.1 | Observations

Over the total monitoring period, stations RFID 3 and RFID 2 recorded 31 and six tracer passages, respectively (Table 1 and Figure 3), with the six tracers detected by RFID 2 also being detected by RFID 3. These 37 observations were then included in the following analysis, with the six observations made by RFID 2 being considered as distinct observations to those made by RFID 3. Among the 31 tracers detected, 29 were injected in 2020, including 14 injected at *INJ 2* (1.2 km upstream of the station *RFID 3*), 14 injected at *INJ 5* (275 m upstream of the permanent RFID station), and 1 injected at *INJ 4* (about 225 m upstream of the RFID stations—Figure 1). Two detected tracers were injected in 2019 at location *INJ 1*, the most upstream point (3.5 km upstream of station *RFID 3*). It should be noted that of the tracers located upstream before the monitoring period and then located downstream in the tracer inventories performed after the monitoring period, all were sensed by the station.

The average *b*-axis, weight, and sphericity of the tracers were 59 mm, 0.265 kg, and 0.73, respectively (Figure 4). The residence time within the RFID station sensing fields ranged from 36 s to 8.8 days, corresponding to virtual velocities of $2.01 (\pm 0.18)$ to $7.9 \times 10^{-5} (\pm 0.03) \text{ m s}^{-1}$ (i.e. 6.8 m day^{-1}), with both extremes being recorded by the permanent station. The absolute and relative uncertainty ranged from 0.18 to 0.03 m s^{-1} and from 42% to $2.6 \times 10^{-4}\%$, respectively. Of the 37 passages, 26 occurred during snowmelt-driven flood events (before mid-July) with mean discharges ranging from 11.3 to $22.5 \text{ m}^3 \text{ s}^{-1}$. The remaining 11 passages occurred during rainfall-driven flood events, with mean discharges varying between 6.1 m and

$70 \text{ m}^3 \text{ s}^{-1}$ (the latter was observed during the peak of a flood event with an estimated return period of 30 years). The seismic activity recorded during the tracer passages ranged from 0.003 to 0.055 mV over periods of snowmelt-driven flows, and from 0.002 to 0.27 mV over rainfall-driven flows (Figure 3). Over these two periods, the virtual velocities ranged from 0.007 to 0.095 m s^{-1} for snowmelt-driven flows and from 0.002 to 2.01 m s^{-1} for rainfall-driven flows. Thus, we observed particle motion under contrasting flow conditions, for different tracer properties and for different passage velocities.

4.2 | Virtual particle velocity as a function of a single controlling variable

We found positive power correlations between logged values of the tracer virtual velocities and logged mean discharges ($R^2 = 0.58$; p -value < 0.001) and logged dimensionless mean stream power ($R^2 = 0.63$; p -value < 0.001). The correlations were even stronger between the logged mean tracer velocities and logged mean seismic activity ($R^2 = 0.81$; p -value < 0.001 ; Figure 6). The logged sum of excess stream power exhibited weak negative power correlations ($R^2 = 0.21$; p -value = $0.83 > 0.05$) with tracer virtual velocities. The log-log power law linking tracer virtual velocities to dimensionless mean stream power exhibited a factor (9.7) very close to that of the log-log power law linking tracer virtual velocities to mean seismic activity (9.4). However, its exponent coefficient (4.1) was very close to that of the log-log power law linking mean flow discharges and virtual velocity (4), which is unsurprising, as dimensionless mean stream power is based on mean discharge. Except for the sum of excess stream power, most of the data scattered around the regression

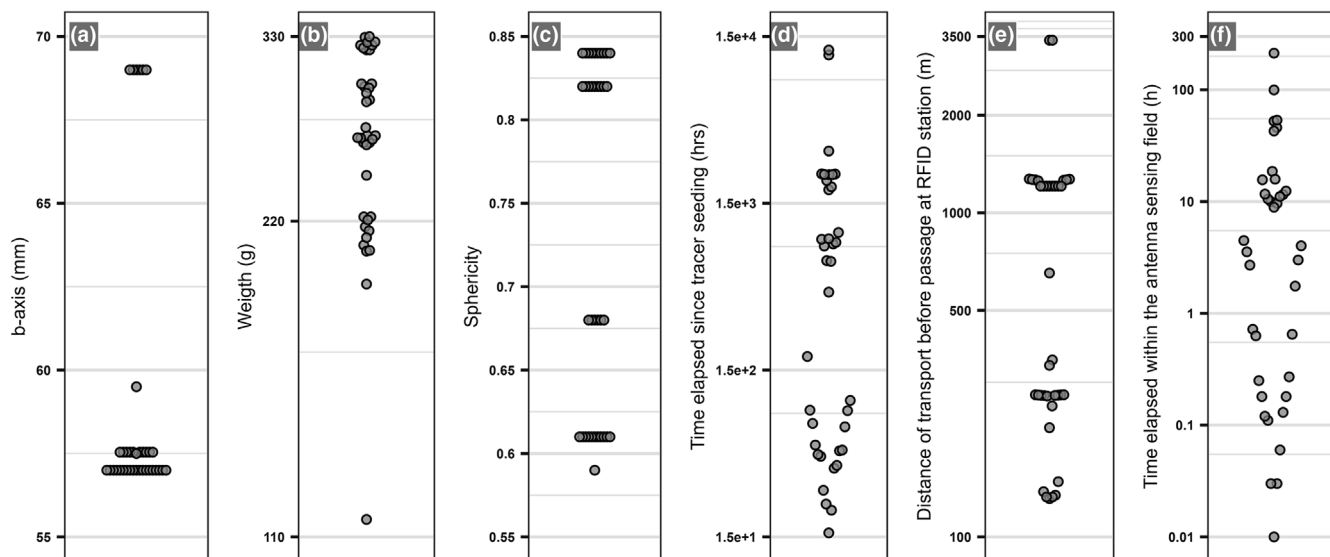
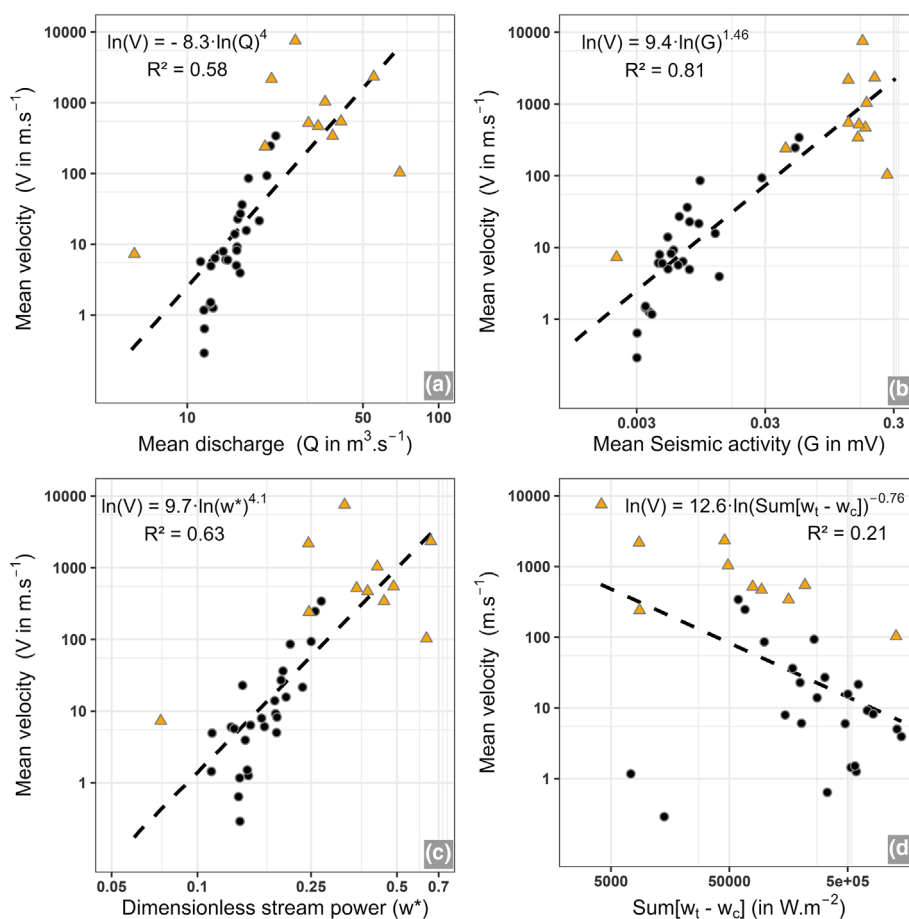


FIGURE 4 Swarm plot of the distributions of the 37 tracer passages recorded: (a) b-axis, (b) weight, (c) sphericity, (d) dwell time in the RFID antenna sensing fields, (e) time elapsed since injection before tracer passage at the RFID stations and (f) distance of travel.

FIGURE 5 Relationships between logged tracer virtual velocity and the mean values of (a) logged flow discharge, (b) logged seismic activity, (c) logged dimensionless mean stream power, and (d) logged the sum of excess flow power per unit area. Notes: circles and triangles represent the passages observed during snowmelt events and storm events, respectively. [Color figure can be viewed at wileyonlinelibrary.com]



curves were for low or high virtual velocity values, whereas dispersion remained relatively moderate for medium values (Figure 6).

The tracer passages occurring during storm events showed higher mean particle velocities, higher flow discharges and higher seismic activity than those during the snowmelt period (Figure 5). The power regression curves among the logged tracer virtual velocity (\bar{v}_P) and the logged mean flow discharges (Figure 5a), logged dimensionless

mean stream power (Figure 5c), and logged average seismic activity (Figure 5b) show wider dispersion for storm events than for snowmelt ones.

We also found that averaged seismic activity showed strong positive power correlations with mean flow discharge ($R^2 = 0.83$; p -value < 0.001; spearman correlation = 0.93) and dimensionless mean stream power ($R^2 = 0.81$; p -value < 0.001; spearman

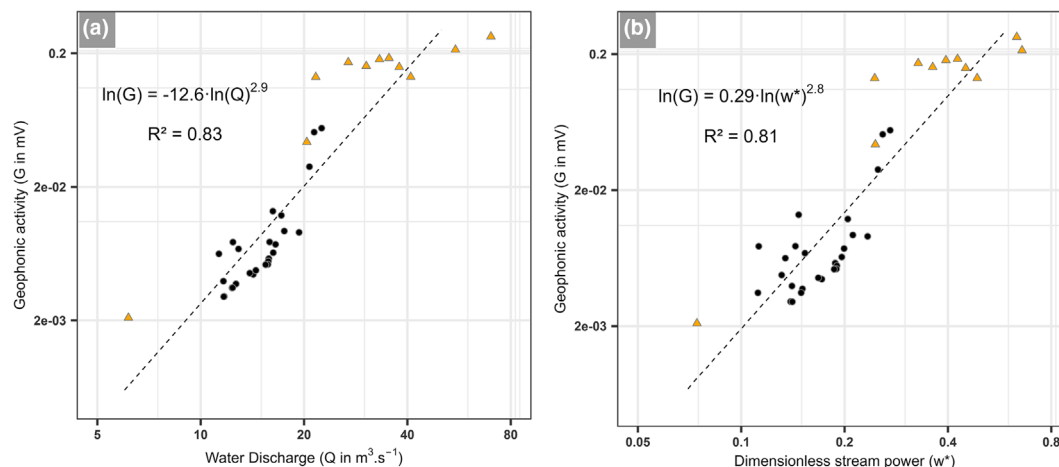


FIGURE 6 Relationships between (a) logged mean geophonic activity and logged mean discharge, and (b) logged dimensionless stream power. Notes: circles and triangles represent the passages observed during snowmelt events and storm events, respectively. [Color figure can be viewed at wileyonlinelibrary.com]

TABLE 3 Results of the multiple regression analysis using a stepwise procedure.

Variable	Coefficient	p-value	Percent of variance explained
Intercept	6.841	4.01e ⁻⁰⁶ ***	
$\ln(\bar{G}_i)$	1.475	4.01e ⁻¹⁶ ***	81.6
$\ln(m_i)$	-3.486	9.8e ⁻⁰⁴ ***	0.22
$\ln(\psi_i)$	6.443	6.85e ⁻⁰⁵ ***	6.99

Notes: Residual standard error: 0.893 with 33 degrees of freedom. Multiple $R^2 = 0.890$. Adjusted $R^2 = 0.877$. F-statistic: 64.98 with 4 and 32 degrees of freedom. p-value = 6.3e-16.

***p-value statistically significant at a 99% confidence level.

correlation = 0.87; Figure 6), which supports the use of the residuals (ϵ_i) from the log-log power model linking log transformed dimensionless mean stream power and log transformed averaged seismic values.

4.3 | Multiple regression analysis

The results of the multiple regression analysis show a highly significant relationship between tracer virtual velocity and independent variables ($R^2 = 0.891$; p-value < 0.001). The seismic activity (\bar{G}_i) explained 81.6% of variance. From the tracer properties tested, the stepwise procedure selected sphericity (ψ_i) and weight (m_i), which explained 5.8% and 0.01% of the virtual velocity variance, respectively. ϵ_i , the residuals from the power model linking log transformed dimensionless mean stream power (w^*) and log transformed seismic averaged values (\bar{G}), were not contributive (p-value > 0.05) (Table 3).

The data scattering around the 1:1 line is moderate and relatively homogeneous between low, medium, and high virtual velocity values (Figure 7). Equation 4 was adapted to estimate the tracer virtual velocity observed within the studied reach for both storm events and snowmelt events (Figure 7).

$$\ln(\bar{v}_p) = 6.84 \cdot \ln(\bar{G}_i)^{1.47} \cdot \ln(m_i)^{-3.48} \cdot \ln(\psi_i)^{6.44} \quad (4)$$

Of the 37 values modelled, all were within a tenfold interval of the observed values, and only 9 (24%) were found to deviate by more than a

factor of 2. We found in the relationship between observed and predicted values associated with the different RFID monitoring stations.

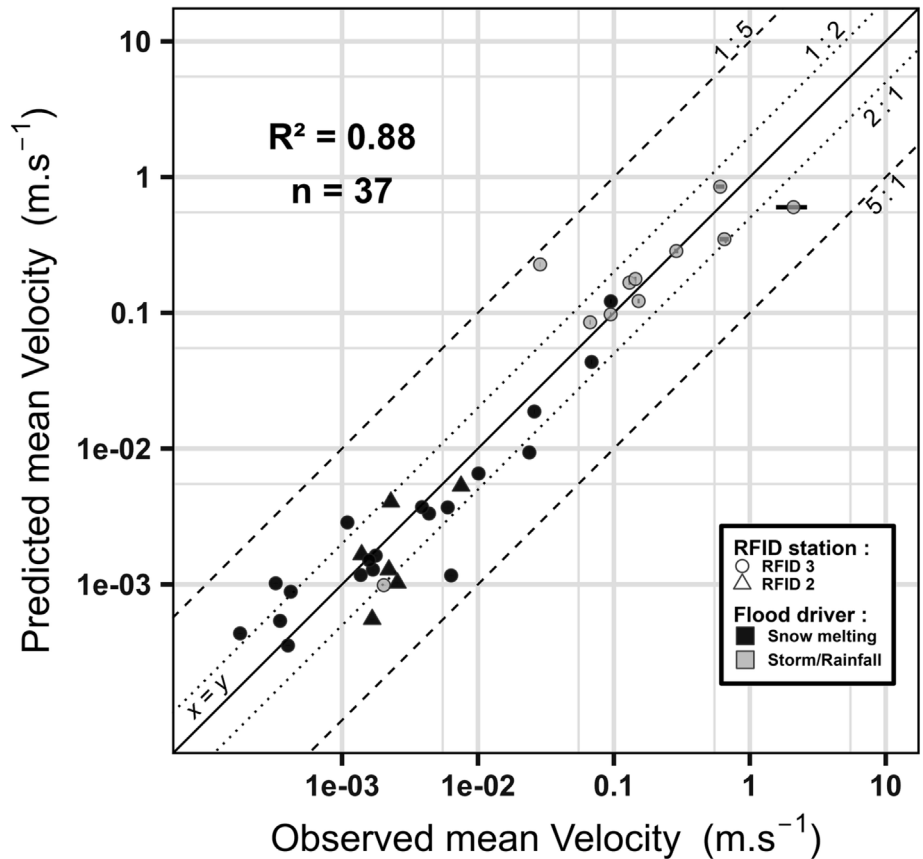
5 | DISCUSSION

5.1 | Field observations and monitoring

Altogether, we recorded 37 tracer passages recorded at two RFID stations. This is close to the number reported by Liedermann et al. (2013) and Klösch & Habersack (2018). Although, this number may seem small, it is typical of this type of experimental setting. The tracers were injected at five distant injections points, on different dates (including a year prior to the monitoring period) and at contrasting flow stages. Thus, even though the tracers were dropped into the river, we assumed that the time elapsed and travel distance before their passages past station RFID2 attenuated the effect of injection mode. However, future experiments could test the effect of different injection modes, locations and flow stages.

The virtual velocities (\bar{v}_p) reported in this study ranged between 0.29 and 7548 m h^{-1} , with mean and median values of 440 and 15.7 m h^{-1} , respectively. Most of the values are within the range of those observed on comparable river systems by Missot et al. (2020), but at larger temporal and spatial scales, with the authors reporting virtual velocities between 13 and 27 m h^{-1} on a 'braided-confined-braided' sequence of the Séveraise River. Liébault et al. (2012) reported values of about 100 m h^{-1} for several grain sizes monitored in a wandering mountain stream. However, the virtual velocities reported in this paper

FIGURE 7 Comparison between the observed and predicted virtual velocity of tracer passages. Notes: dashed and dotted lines indicate the tenfold and twofold intervals, respectively. Uncertainty of measured values are shown when longer than the points.



are higher than those observed on the alpine headwater streams of the Rio Cordon, where virtual velocities were globally less than 6 m h^{-1} (Mao et al., 2017; Oss Cazzador et al., 2021; Rainato et al., 2020). Although our observations are higher, they are generally less than the 60 m h^{-1} reported by Dell'Agnese et al. (2015), who also reported that higher virtual velocity was associated more with rainfall-dominated periods than with snowmelt and mixed periods.

The fastest virtual velocity we measured was 2.01 m s^{-1} over a step length 60 m , which was probably the closest to the instantaneous velocity. This value is impressive but consistent with previous observations and measured flow velocities. Indeed, Habersack (2001) observed a maximum instantaneous particle velocity of 2 m s^{-1} and a maximal individual step length of 24.9 m on a braided reach. It is reasonable to hypothesise that the geometry of the straight confined channel of our study site allowed for a longer individual step length compared with that generally observed on a braided reach. The tracer virtual velocity value is also consistent with the flow velocity of 2.7 m s^{-1} estimated at the mean discharge value of $27 \text{ m}^3 \text{ s}^{-1}$ that was measured during its passage.

The estimated critical discharge for bedload transport (Q_c) was $11.9 \text{ m}^3 \text{ s}^{-1}$. This value is consistent with the tracer passages observed in the early stage of the snow melt season up until the flood events of 1 and 2 July, with peak flow discharges of 28 and $21.5 \text{ m}^3 \text{ s}^{-1}$, respectively (Figure 3). Prior to these flood events, the tracers passing through the RFID station sensing field with discharge values (\bar{Q}_i) very close to Q_c (i.e. from 11.6 to $12.7 \text{ m}^3 \text{ s}^{-1}$) exhibited the lowest virtual velocities (from 0.29 to 1.5 m h^{-1}). After the 1 and 2 July flood events, this threshold was no longer so clear. Indeed, the tracers that passed through the station sensing field at $\bar{Q}_i \approx Q_c$ exhibited more varied residence times within the antenna sensing field (i.e. 9.6 , 11.1 , 12.4 , and 53 h) and exhibited three-times higher \bar{v}

values (i.e. 6.3 , 5.7 , 4.9 , and 1.2 m h^{-1} , respectively) at equivalent \bar{Q}_i values (i.e. 12.9 , 11.3 , 12.4 , and $11.6 \text{ m}^3 \text{ s}^{-1}$, respectively) than the tracers monitored before the 1 and 2 July flood events. Over the post-flood-event period, there was a temporary increase in seismic activity that lasted until 6 July, although flow discharges were slightly lower than in the pre-flood-event period (Figure 3). These observations can be interpreted in two ways: as a limitation of Q_c calculations (using Shields number in our case) that transcribe a section of averaged particle bed behavior and can at some scale misestimate the local conditions surrounding some tracers, or they can be attributed to the effects of the antecedent geomorphological conditions on tracer passage dynamics. Indeed, breaking of the armor layer, channel shifting (especially in river systems as dynamic as braided streams), and ongoing channel adjustment after a major flood can locally and temporarily promote bedload particle transport. Such delayed bedload transport processes following a flood event were reported by Aigner et al. (2017) using a geophone plate but remain difficult to observe with sediment tracers, although they do demonstrate the complementarity of geophones and tracer tools. This is an important topic that could provide information useful for understanding the passage of tracers observed at the lowest average discharge value $\bar{Q}_i = 6.2 \text{ m}^3 \text{ s}^{-1}$, which is well below the Q_c , but still at a virtual velocity of $\bar{v} = 7.3 \text{ m h}^{-1}$.

5.2 | Drivers of particle motion and prediction of virtual mobility

Although Figure 5d shows a marked segregation relative to flood event types, the statistical relationship between the sum of excess

stream power and virtual velocities exhibited weak negative power correlations ($R^2 = 0.21$; p -value = $0.83 > 0.05$). This negative correlation, consistent with that in previous work by Chardon et al. (2021), can be attributed to the fact that both virtual velocity and cumulative excess stream power are dependent on time, the first being negatively correlated (i.e. the shorter the time spent in the antenna sensing field, the higher the virtual velocity) and the second positively correlated (i.e. the longer the time spent, the higher the cumulative excess stream power). Thus, cumulative excess stream power is more suitable for investigating cumulative transport distances than for investigating virtual velocity.

Furthermore, the percentage of mean tracer velocity variance explained by the seismic signals was higher than that explained by flow discharges (Figure 5a,b). The two are strongly correlated (Figure 6), and the geophone activity integrates some of the virtual velocity variance explained by flow discharge. Thus, compared with the single flow discharge, the seismic signal, as an integrated measure of flow conditions and bedload transport, explains a larger amount of the variance in the coarse-particle virtual velocities and offers a better way to predict bedload velocities in a confined channel. The link between virtual velocity and seismic signal is consistent with the results of Schneider et al. (2014), who reported a strong link between unit bed load volume and the mean distance of tracer transport. Both their results and those we report here support the use of tracers together with measurements of the scour layer thickness made by classical or RFID scour chains (Boutault, 2020; Brenna et al., 2019; Laronne et al., 1994; Liébault & Laronne, 2008; Melun et al., 2019) to quantify bedload transport flux in rivers where direct sampling is not feasible.

The overall variance of mean tracer velocities explained by particle properties was about 7%, most of it being explained by sphericity (6.99%), which exhibited a positive coefficient and contributed to explaining particle velocity. This is consistent with previous in-flume tracking experiments (Cassel, Lavé, et al., 2021). Moreover, the particle weight explained much less of the variance (0.22%) and contributed negatively to virtual velocity. Future work should investigate and compare the coefficients for the controlling variables resulting from the multiple regression analysis with those obtained in river systems of contrasting morphologies. Indeed, it is reasonable to assume that in river systems exhibiting less torrential processes, the proportion of particle virtual velocity variance explained by the seismic activity signal could be lower. Finally, the acquisition of more observations would allow expansion of the statistical sample and allow analysis of the effects of more control variables using a similar stepwise procedure to that used by Vázquez-Tarrió & Batalla (2019). Further comparisons are needed to determine if such methodology would allow assessment of whether or not the interactions between moving particles influence their mobility (entrainment, motion and deposition), and to what extent compared with flow discharge.

5.3 | About the combination of Lagrangian and Eulerian approaches

In this study, we proposed in-field technical solutions and an empirical model that allows merging Lagrangian and Eulerian

descriptions of bedload transport, which is illustrated with a study case of the Severaisse River, France. This led the way to further experiments and/or developments. First, it would be relevant to increase the number of tracers and to expand the range of grain sizes, thereby strengthening the models. Second, the spatial domains could be expanded, initially remaining within a reach with homogeneous morphologic characteristics. This could be performed by installing several RFID and geophone stations (one at the upstream bound, one in the middle and a third at the downstream bound) along the selected river reach. This would allow description of the propagation of bedload fluctuations according to both fluxes and particle measurements. Third, tracer movements measurements with finer spatial and temporal resolutions would allow estimation of the instantaneous velocity, instead of virtual velocity, and would thus provide more accurate calculations of the impact energy that could be linked with the seismic activity sensed at the same moment. This last point would require technical solutions for accurate timestamp matching of the Lagrangian and Eulerian observations. This would also be a step for the use of the Kalinske's mechanical approach (sediment transport rate been the product of particle activity and velocity) to estimate sediment flux. However, this would require to measure the particle activity as defined by Kalinske (1947) in Ancey (2020a), which remains challenging in the field.

Finally, from a more conceptual point of view, it is possible to consider both $\bar{v} = f(\bar{G})$ (i.e. particle motion predicted from flux, plus their intrinsic properties) and $\bar{G} = f(\bar{v})$ (i.e. flux as a function of particle motion) as transfer functions. The first allows prediction of \bar{v} (and estimation of the tracers' transport distance and dispersion), which requires a great deal of effort to acquire in the field (time consuming and laborious prospections). However, the definition is less useful for obtaining intensity from distance and is not as practical because the transport distance is laborious to measure in the field and the intensity still needs to be calibrated with field measurements of bedload transport.

6 | CONCLUSIONS

The e-RFIDuino station showed good efficiency for monitoring the passage of tracers in a diversity of flood events and associated hydraulic conditions. It also has important potential for the study of the phases of bedload transport at the particle scale. The combination of RFID and geophone environmental stations allowed surveying of tracer passages and seismic activity over a period of several months, and facilitated detection of shifts in river system dynamics in pre- and post-flood analyses. The comparison of the efficiencies of flow discharge and seismic activity for predicting the virtual velocity of tracers showed that seismic activity, as for suspended load prediction (Misset et al., 2021), is a better predictive factor than flow discharge. The results of the multiple regression analysis also confirmed, in-river, the contribution of the particle shape to the observed virtual velocity. Further investigations in different river systems with finer granulometry and/or a larger channel and/or more fluvial and less torrential dynamics are needed to specify the potential of such a monitoring setup and to achieve insights into the relationships between grain-scale processes and bulk bedload transport.

ACKNOWLEDGEMENTS

The authors thank the electricity company Électricité de France (EDF), who provided us with the discharge values measured at its gauging station. Léonie Besson and Nils Dumarski are acknowledged for their participation in the e-RFIDuino station installation and sensing field delineation during field campaigns. The authors thank the OMEAA research platform supported by the University Lumière Lyon and the CNRS for the laboratory analyses and/or field measurements and Franck Perret for the e-RFIDuino station. The authors thank Karl Embleton for his proofreading work. Thanks are also extended to Editor Stuart Lane and Executive Editor of ESPL journal. Finally, the authors thank the two anonymous reviewers whose remarks helped us to improve this article.

This work was performed within the framework of the EUR H2O'Lyon (ANR-17-EURE-0018) of Université de Lyon, part of the programme 'Investissements d'Avenir' (ANR-11-IDEX-0007) operated by the French National Research Agency (ANR).

This work was carried out as part of the project **Greendam**, which is an original partnership integrating an inter-disciplinary scientific group (EVS UMR 5600 and SiSyPh UMR5672 du CNRS et INRAE), a large electricity producer (Électricité de France - EDF), and a local SME (GeoPeka), as part of a partnership project with the Région Auvergne-Rhône-Alpes.

CONFLICT OF INTEREST STATEMENT

The authors declare no competing interests.

DATA AVAILABILITY STATEMENT

Data are not available.

STATEMENT OF HUMAN AND ANIMAL RIGHTS

The authors declare that no human or animal subjects were used in this study.

ORCID

Mathieu Cassel  <https://orcid.org/0000-0001-6504-3990>

Oldrich Navratil  <https://orcid.org/0000-0002-3464-6366>

Frédéric Liébault  <https://orcid.org/0000-0002-3155-6779>

Alain Recking  <https://orcid.org/0000-0003-3278-4463>

Daniel Vázquez-Tarrío  <https://orcid.org/0000-0002-5658-4426>

Maarten Bakker  <https://orcid.org/0000-0001-5658-1690>

Hervé Piégay  <https://orcid.org/0000-0002-3864-2119>

REFERENCES

- Aigner, J., Kreisler, A., Rindler, R., Hauer, C. & Habersack, H. (2017) Bedload pulses in a hydropower affected alpine gravel bed river. *Geomorphology*, 291, 116–127. Available from: <https://doi.org/10.1016/j.geomorph.2016.05.015>
- Ancey, C. (2020a) Bedload transport: a walk between randomness and determinism. Part 1. The state of the art. *Journal of Hydraulic Research*, 58(1), 1–17. Available from: <https://doi.org/10.1080/00221686.2019.1702594>
- Ancey, C. (2020b) Bedload transport: a walk between randomness and determinism. Part 2. Challenges and prospects. *Journal of Hydraulic Research*, 58(1), 18–33. Available from: <https://doi.org/10.1080/00221686.2019.1702595>
- Antoniazza, G., Nicollier, T., Wyss, C.R., Boss, S. & Rickenmann, D. (2020) Bedload transport monitoring in Alpine Rivers: variability in Swiss plate geophone response. *Sensors*, 20(15), 4089. Available from: <https://doi.org/10.3390/s20154089>
- Arnaud, F., Piégay, H., Béal, D., Coltery, P., Vaudor, L. & Rollet, A.-J. (2017) Monitoring gravel augmentation in a large regulated river and implications for process-based restoration. *Earth Surface Processes and Landforms*, 42(13), 2147–2166. Available from: <https://doi.org/10.1002/esp.4161>
- Bagnold, R.A. (1966) *An approach to the sediment transport problem from general physics*. USGS Numbered Series. Washington: U.S. Government Printing Office [online]. Available from: <http://pubs.er.usgs.gov/publication/pp4221> [Accessed 21 November 2018].
- Bagnold, R.A. (1980) An empirical correlation of bedload transport rates in flumes and natural rivers. *Proceedings of the Royal Society A: Mathematical, Physical and Engineering Sciences*, 372(1751), 453–473. Available from: <https://doi.org/10.1098/rspa.1980.0122>
- Bakker, M., Gimbert, F., Geay, T., Misset, C., Zanker, S. & Recking, A. (2020) Field application and validation of a seismic bedload transport model. *Journal of Geophysical Research - Earth Surface*, 125(5), e2019JF005416. Available from: <https://doi.org/10.1029/2019JF005416>
- Ballio, F., Pokrajac, D., Radice, A. & Hosseini Sadabadi, S.A. (2018) Lagrangian and Eulerian description of bed load transport. *Journal of Geophysical Research - Earth Surface*, 123(2), 384–408. Available from: <https://doi.org/10.1002/2016JF004087>
- Bel, C., Liébault, F., Navratil, O., Eckert, N., Bellot, H., Fontaine, F., et al. (2017) Rainfall control of debris-flow triggering in the réal torrent, southern French Prealps. *Geomorphology*, 291, 17–32. Available from: <https://doi.org/10.1016/j.geomorph.2016.04.004>
- Boutault, F. (2020) Etude de l'impact cumulé des facteurs d'anthropisation sur la Dordogne moyenne et préconisations en vue d'une restauration écologique du cours d'eau. Géographie. Université Jean-Moulin (Lyon 3), Français.
- Bradley, D.N. (2017) Direct observation of heavy-tailed storage times of bed load tracer particles causing anomalous superdiffusion. *Geophysical Research Letters*, 44(24), 12,227–12,235. Available from: <https://doi.org/10.1002/2017GL075045>
- Brenna, A., Surian, N. & Mao, L. (2019) Virtual velocity approach for estimating bed material transport in gravel-bed rivers: key factors and significance. *Water Resources Research*, 55(2), 1651–1674. Available from: <https://doi.org/10.1029/2018WR023556>
- Brousse, G., Arnaud-Fassetta, G., Liébault, F., Bertrand, M., Melun, G., Loire, R. et al. (2020) Channel response to sediment replenishment in a large gravel-bed river: the case of the Saint-Sauveur dam in the Buëch River (Southern Alps, France). *River Research and Applications*, 36(6), rra.3527. Available from: <https://doi.org/10.1002/rra.3527>
- Brousse, G., Liébault, F., Arnaud-Fassetta, G., Breilh, B. & Tacon, S. (2020) Gravel replenishment and active-channel widening for braided-river restoration: the case of the upper Drac River (France). *Science of the Total Environment*, 766, 142517. Available from: <https://doi.org/10.1016/j.scitotenv.2020.142517>
- Cassel, M., Dépret, T. & Piégay, H. (2017) Assessment of a new solution for tracking pebbles in rivers based on active RFID: a new solution for tracking pebbles in rivers based on active RFID. *Earth Surface Processes and Landforms*, 42(13), 1938–1951. Available from: <https://doi.org/10.1002/esp.4152>
- Cassel, M., Lavé, J., Recking, A., Malavoi, J.-R. & Piégay, H. (2021) Bedload transport in rivers, size matters but so does shape. *Scientific Reports*, 11(1), 508. Available from: <https://doi.org/10.1038/s41598-020-79930-7>
- Cassel, M., Navratil, O., Perret, F. & Piégay, H. (2021) The e-RFIDuino: an Arduino-based RFID environmental station to monitor mobile tags. *HardwareX*, 10, e00210. Available from: <https://doi.org/10.1016/j.ohx.2021.e00210>
- Cassel, M., Piégay, H., Fantino, G., Lejot, J., Bultingaire, L., Michel, K. et al. (2020) Comparison of ground-based and UAV a-UHF artificial tracer mobility monitoring methods on a braided river. *Earth Surface Processes and Landforms*, 45, 1123–1140. Available from: <https://doi.org/10.1002/esp.4777>
- Cassel, M., Piégay, H. & Lavé, J. (2017) Effects of transport and insertion of radio frequency identification (RFID) transponders on resistance and shape of natural and synthetic pebbles: applications for riverine and coastal bedload tracking. *Earth Surface Processes and Landforms*, 42, 399–413. Available from: <https://doi.org/10.1002/esp.3989>

- Chardon, V., Schmitt, L., Arnaud, F., Piégay, H. & Clutier, A. (2021) Efficiency and sustainability of gravel augmentation to restore large regulated rivers: insights from three experiments on the Rhine River (France/Germany). *Geomorphology*, 380, 107639. Available from: <https://doi.org/10.1016/j.geomorph.2021.107639>
- Cook, K.L., Andermann, C., Gimbert, F., Adhikari, B.R. & Hovius, N. (2018) Glacial lake outburst floods as drivers of fluvial erosion in the Himalaya. *Science*, 362(6410), 53–57. Available from: <https://doi.org/10.1126/science.aat4981>
- Dell'Agnese, A., Brardinoni, F., Toro, M., Mao, L., Engel, M. & Comiti, F. (2015) Bedload transport in a formerly glaciated mountain catchment constrained by particle tracking. *Earth Surface Dynamics*, 3(4), 527–542. Available from: <https://doi.org/10.5194/esurf-3-527-2015>
- Dietze, M., Lagarde, S., Halfi, E., Laronne, J.B. & Turowski, J.M. (2019) Joint sensing of bedload flux and water depth by seismic data inversion. *Water Resources Research*, 55(11), 9892–9904. Available from: <https://doi.org/10.1029/2019WR026072>
- Dietze, M., Losee, J., Polvi, L. & Palm, D. (2020) A seismic monitoring approach to detect and quantify river sediment mobilization by steel-head redd-building activity. *Earth Surface Processes and Landforms*, 45(12), 2840–2849. Available from: <https://doi.org/10.1002/esp.4933>
- Eaton, B.C. & Church, M. (2011) A rational sediment transport scaling relation based on dimensionless stream power. *Earth Surface Processes and Landforms*, 36(7), 901–910. Available from: <https://doi.org/10.1002/esp.2120>
- Einstein, H. (1937) *Der Geschiebetrieb als Wahrscheinlichkeitproblem (Bedload transport as a probability problem)* (English translation by W. W. Sayre, in Sedimentation (Symposium to honor H. A. Einstein). In: Shen, H. W. (Ed.), Fort Collins, Colorado, 1972, C1–C105). Zurich: ETHZ.
- Ergenzinger, P. & Schmidt, K.H. (1990) Stochastic elements of bed load transport in a steppool mountain river. Hydrology in mountainous regions. II—Artificial reservoirs, water and slopes. *International Association of Hydrological Sciences Publication*, 194, 39–46.
- Frey, P. & Church, M. (2011) Bedload: a granular phenomenon. *Earth Surface Processes and Landforms*, 36(1), 58–69. Available from: <https://doi.org/10.1002/esp.2103>
- Gilet, L., Gob, F., Gautier, E., Houbrechts, G., Vermoux, C. & Thommeret, N. (2020) Hydro-morphometric parameters controlling travel distance of pebbles and cobbles in three gravel bed streams. *Geomorphology*, 358, 107117. Available from: <https://doi.org/10.1016/j.geomorph.2020.107117>
- Gimbert, F., Fuller, B.M., Lamb, M.P., Tsai, V.C. & Johnson, J.P.L. (2019) Particle transport mechanics and induced seismic noise in steep flume experiments with accelerometer-embedded tracers. *Earth Surface Processes and Landforms*, 44(1), 219–241. Available from: <https://doi.org/10.1002/esp.4495>
- Gomez, B. (1991) Bedload transport. *Earth-Science Reviews*, 31(2), 89–132. Available from: [https://doi.org/10.1016/0012-8252\(91\)90017-A](https://doi.org/10.1016/0012-8252(91)90017-A)
- Habersack, H., Seitz, H. & Liedermann, M. (2010) Integrated automatic bedload transport monitoring. *US Geological Survey Scientific Investigations Report*, 5091, 218–235.
- Habersack, H.M. (2001) Radio-tracking gravel particles in a large braided river in New Zealand: a field test of the stochastic theory of bed load transport proposed by Einstein. *Hydrological Processes*, 15(3), 377–391. Available from: <https://doi.org/10.1002/hyp.147>
- Haschenburger, J.K. (2013) Tracing river gravels: insights into dispersion from a long-term field experiment. *Geomorphology*, 200, 121–131. Available from: <https://doi.org/10.1016/j.geomorph.2013.03.033>
- Haschenburger, J.K. & Church, M. (1998) Bed material transport estimated from the virtual velocity of sediment. *Earth Surface Processes and Landforms*, 23(9), 791–808. Available from: [https://doi.org/10.1002/\(SICI\)1096-9837\(199809\)23:9<791::AID-ESP888>3.0.CO;2-X](https://doi.org/10.1002/(SICI)1096-9837(199809)23:9<791::AID-ESP888>3.0.CO;2-X)
- Haschenburger, J.K. & Wilcock, P.R. (2003) Partial transport in a natural gravel bed channel: transport in a gravel bed channel. *Water Resources Research*, 39(1), n/a–n/a. Available from: <https://doi.org/10.1029/2002WR001532>
- Hassan, M.A. & Bradley, D.N. (2017) In: Rivers, G.-B., Tsutsumi, D. & Laronne, J.B. (Eds.) *Geomorphic controls on tracer particle dispersion in gravel-bed rivers*. Chichester, UK: John Wiley & Sons, Ltd, pp. 159–184. [online] Available from: <http://doi.wiley.com/10.1002/9781118971437.ch6> [Accessed 29 April 2020].
- Houbrechts, G., Levecq, Y., Peeters, A., Hallot, E., Van Campenhout, J., Denis, A.-C. et al. (2015) Evaluation of long-term bedload virtual velocity in gravel-bed rivers (Ardenne, Belgium). *Geomorphology*, 251, 6–19. Available from: <https://doi.org/10.1016/j.geomorph.2015.05.012>
- Imhoff, K.S. & Wilcox, A.C. (2016) Coarse bedload routing and dispersion through tributary confluences. *Earth Surface Dynamics*, 4(3), 591–605. Available from: <https://doi.org/10.5194/esurf-4-591-2016>
- Kalinske, A.A. (1947) Movement of sediment as bed load in rivers. *Transactions of the American Geophysical Union*, 28(4), 615. Available from: <https://doi.org/10.1029/TR028i004p0615>
- Klößch, M. & Habersack, H. (2018) Deriving formulas for an unsteady virtual velocity of bedload tracers. *Earth Surface Processes and Landforms*, 43, 1529–1541. Available from: <https://doi.org/10.1002/esp.4326>
- Kondolf, G.M. & Piégay, H. (2016) Tools in fluvial geomorphology: problem statement and recent practice. In: Gthias, K. & Piégay, H. (Eds.) *Tools in fluvial geomorphology*. John Wiley & Sons, Ltd, pp. 1–12. [online] Available from: <http://onlinelibrary.wiley.com/doi/10.1002/9781118648551.ch1/summary> [Accessed 2 November 2016].
- Lamarre, H. & Roy, A.G. (2008) The role of morphology on the displacement of particles in a step-pool river system. *Geomorphology*, 99(1–4), 270–279. Available from: <https://doi.org/10.1016/j.geomorph.2007.11.005>
- Laronne, J.B., Outhet, D.N., Carling, P.A. & McCabe, T.J. (1994) Scour chain employment in gravel bed rivers. *Catena*, 22(4), 299–306. Available from: [https://doi.org/10.1016/0341-8162\(94\)90040-X](https://doi.org/10.1016/0341-8162(94)90040-X)
- Liébault, F., Bellot, H., Chapuis, M., Klotz, S. & Deschâtres, M. (2012) Bedload tracing in a high-sediment-load mountain stream: bedload tracing in a high-sediment-load mountain stream. *Earth Surface Processes and Landforms*, 37(4), 385–399. Available from: <https://doi.org/10.1002/esp.2245>
- Liébault, F. & Laronne, J.B. (2008) Evaluation of bedload yield in gravel-bed rivers using scour chains and painted tracers: the case of the Esconavette torrent (southern French Prealps). *Geodinamica Acta*, 21(1–2), 23–34. Available from: <https://doi.org/10.3166/ga.21.23-34>
- Liedermann, M., Tritthart, M. & Habersack, H. (2013) Particle path characteristics at the large gravel-bed river Danube: results from a tracer study and numerical modelling. *Earth Surface Processes and Landforms*, 38(5), 512–522. Available from: <https://doi.org/10.1002/esp.3338>
- Mao, L., Dell'Agnese, A. & Comiti, F. (2017) Sediment motion and velocity in a glacier-fed stream. *Geomorphology*, 291, 69–79. Available from: <https://doi.org/10.1016/j.geomorph.2016.09.008>
- McDowell, C. & Hassan, M.A. (2020) The influence of channel morphology on bedload path lengths: insights from a survival process model. *Earth Surface Processes and Landforms*, 45(12), 2982–2997. Available from: <https://doi.org/10.1002/esp.4946>
- Melun, G., Arnaud, F., Arnaud-Fassetta, G., Bertrand, M., Bilodeau, C., Borgniet, L. et al. (2019) Dossier: L'hydromorphologie. *La Houille Blanche*, 105(2), 5–25. Available from: <https://doi.org/10.1051/lhb/2019037>
- Misset, C., Recking, A., Legout, C., Bakker, M., Bodereau, N., Borgniet, L. et al. (2020) Combining multi-physical measurements to quantify bedload transport and morphodynamics interactions in an Alpine braiding river reach. *Geomorphology*, 351, 106877. Available from: <https://doi.org/10.1016/j.geomorph.2019.106877>
- Misset, C., Recking, A., Legout, C., Bakker, M., Gimbert, F., Geay, T. et al. (2021) Using continuous turbidity and seismic measurements to unravel sediment provenance and interaction between suspended and bedload transport in an Alpine catchment. *Geophysical Research Letters*, 48, e2020GL090696. Available from: <https://doi.org/10.1029/2020GL090696>
- Navratil, O., Liébault, F., Bellot, H., Travaglini, E., Theule, J., Chambon, G. et al. (2013) High-frequency monitoring of debris-flow propagation along the réal torrent, southern French Prealps. *Geomorphology*, 201, 157–171. Available from: <https://doi.org/10.1016/j.geomorph.2013.06.017>

- Olinde, L. & Johnson, J. (2015) Using RFID and accelerometer-embedded tracers to measure probabilities of bed load transport, step lengths, and rest times in a mountain stream. *Water Resources Research*, 51(9), 7572–7589. Available from: <https://doi.org/10.1002/2014wr016120>
- Oss Cazzador, D., Rainato, R., Mao, L., Martini, L. & Picco, L. (2021) Coarse sediment transfer and geomorphic changes in an alpine headwater stream. *Geomorphology*, 376, 107569. Available from: <https://doi.org/10.1016/j.geomorph.2020.107569>
- Papangelakis, E. & Hassan, M.A. (2016) The role of channel morphology on the mobility and dispersion of bed sediment in a small gravel-bed stream. *Earth Surface Processes and Landforms*, 41(15), 2191–2206. Available from: <https://doi.org/10.1002/esp.3980>
- Phillips, C.B. & Jerolmack, D.J. (2014) Dynamics and mechanics of bed-load tracer particles. *Earth Surface Dynamics*, 2(2), 513–530. Available from: <https://doi.org/10.5194/esurf-2-513-2014>
- Phillips, C.B., Martin, R.L. & Jerolmack, D.J. (2013) Impulse framework for unsteady flows reveals superdiffusive bed load transport. *Geophysical Research Letters*, 40(7), 1328–1333. Available from: <https://doi.org/10.1002/grl.50323>
- Rainato, R., Mao, L. & Picco, L. (2020) The effects of low-magnitude flow conditions on bedload mobility in a steep mountain stream. *Geomorphology*, 367, 107345. Available from: <https://doi.org/10.1016/j.geomorph.2020.107345>
- Recking, A. (2013) An analysis of nonlinearity effects on bed load transport prediction: NONLINEARITY AND BED LOAD PREDICTION. *Journal of Geophysical Research - Earth Surface*, 118(3), 1264–1281. Available from: <https://doi.org/10.1002/jgrf.20090>
- Rickenmann, D. (2017) Bed-load transport measurements with geophones and other passive acoustic methods. *Journal of Hydraulic Engineering*, 143(6), 03117004. Available from: [https://doi.org/10.1061/\(ASCE\)HY.1943-7900.0001300](https://doi.org/10.1061/(ASCE)HY.1943-7900.0001300)
- Rickenmann, D., Turowski, J.M., Fritschi, B., Klaiber, A. & Ludwig, A. (2012) Bedload transport measurements at the Erlenbach stream with geophones and automated basket samplers: bedload transport measurements in the Erlenbach. *Earth Surface Processes and Landforms*, 37(9), 1000–1011. Available from: <https://doi.org/10.1002/esp.3225>
- Rickenmann, D., Turowski, J.M., Fritschi, B., Wyss, C., Laronne, J., Barzilai, R. et al. (2014) Bedload transport measurements with impact plate geophones: comparison of sensor calibration in different gravel-bed streams: impact plate geophone calibration. *Earth Surface Processes and Landforms*, 39(7), 928–942. Available from: <https://doi.org/10.1002/esp.3499>
- Roth, D.L., Finnegan, N.J., Brodsky, E.E., Rickenmann, D., Turowski, J.M., Badoux, A. et al. (2017) Bed load transport and boundary roughness changes as competing causes of hysteresis in the relationship between river discharge and seismic amplitude recorded near a steep mountain stream. *Journal of Geophysical Research - Earth Surface*, 122(5), 1182–1200. Available from: <https://doi.org/10.1002/2016JF004062>
- Sayre, W.W. & Hubbell, D.W. (1965) *Transport and dispersion of labeled bed material, North Loup River, Nebraska*. USGS Publications Warehouse. Available from: <https://doi.org/10.3133/pp433C>
- Schmandt, B., Gaeuman, D., Stewart, R., Hansen, S.M., Tsai, V.C. & Smith, J. (2017) Seismic array constraints on reach-scale bedload transport. *Geology*, 45(4), 299–302. Available from: <https://doi.org/10.1130/G38639.1>
- Schneider, J., Hegglin, R., Meier, S., Turowski, J., Nitsche, M. & Rickenmann, D. (2010) Studying sediment transport in mountain rivers by mobile and stationary RFID antennas. In: Ditttrich, K., Koll, A., Aberle, J. & Geisen-Hainer, P. (Eds.) *River flow 2010: proceedings of the 5th international conference on fluvial hydraulics*. Braunschweig, Germany: Bundesanstalt, pp. 1723–1730.
- Schneider, J.M., Turowski, J.M., Rickenmann, D., Hegglin, R., Arrigo, S., Mao, L. et al. (2014) Scaling relationships between bed load volumes, transport distances, and stream power in steep mountain channels: tracer Erlenbach. *Journal of Geophysical Research - Earth Surface*, 119(3), 533–549. Available from: <https://doi.org/10.1002/2013JF002874>
- Shields, A. (1936) *Anwendung der Aehnlichkeitsmechanik und der Turbulenzforschung auf die Geschiebebewegung*. PhD Thesis. Berlin: Technical University Berlin [online]. Available from: <https://repository.tudelft.nl/islandora/object/uuid:61a19716-a994-4942-9906-f680eb9952d6?collection=research> [Accessed 13 September 2017].
- Sneed, E.D. & Folk, R.L. (1958) Pebbles in the lower Colorado River, Texas a study in particle morphogenesis. *The Journal of Geology*, 66(2), 114–150. Available from: <https://doi.org/10.1086/626490>
- Stähly, S., Franca, M.J., Robinson, C.T. & Schleiss, A.J. (2020) Erosion, transport and deposition of a sediment replenishment under flood conditions. *Earth Surface Processes and Landforms*, 45(13), 3354–3367. Available from: <https://doi.org/10.1002/esp.4970>
- Strickler, A. (1923) *Beiträge zur Frage der Geschwindigkeitsformel und der Rauheitszahlen für Ströme*. Bern: Kanäle und geschlossene Leitungen.
- Tsai, V.C., Minchew, B., Lamb, M.P. & Ampuero, J.-P. (2012) A physical model for seismic noise generation from sediment transport in rivers: seismic noise from sediment transport. *Geophysical Research Letters*, 39(2), n/a–n/a. Available from: <https://doi.org/10.1029/2011GL050255>
- Vázquez-Tarrio, D. & Batalla, R.J. (2019) Assessing controls on the displacement of tracers in gravel-bed rivers. *Water*, 11(8), 1598. Available from: <https://doi.org/10.3390/w11081598>
- Vázquez-Tarrio, D., Peeters, A., Cassel, M. & Piégay, H. (2023) Modelling coarse-sediment propagation following gravel augmentation: the case of the Rhône River at Péage-de-Roussillon (France). *Geomorphology*, 428, 108639. Available from: <https://doi.org/10.1016/j.geomorph.2023.108639>
- Vázquez-Tarrio, D., Piqué, G., Vericat, D. & Batalla, R.J. (2021) The active layer in gravel-bed rivers: An empirical appraisal. *Earth Surface Processes and Landforms*, 46, 323–343. Available from: <https://doi.org/10.1002/esp.5027>
- Vázquez-Tarrio, D., Recking, A., Liébault, F., Tal, M. & Menéndez-Duarte, R. (2019) Particle transport in gravel-bed rivers: revisiting passive tracer data. *Earth Surface Processes and Landforms*, 44, 112–128. Available from: <https://doi.org/10.1002/esp.4484>

How to cite this article: Cassel, M., Navratil, O., Liébault, F., Recking, A., Vázquez-Tarrio, D., Bakker, M. et al. (2023) Assessment of pebble virtual velocities by combining active RFID fixed stations with geophones. *Earth Surface Processes and Landforms*, 48(13), 2570–2583. Available from: <https://doi.org/10.1002/esp.5646>